Solid-state impedance spectroscopy studies of dielectric properties and relaxation processes in Na₂O–V₂O₅–Nb₂O₅–P₂O₅ glass system

Sara Marijan and Luka Pavić✉

Division of Materials Chemistry, Ruđer Bošković Institute, Bijenička 54, HR-10000 Zagreb, Croatia
✉ Corresponding author: Luka Pavić   E-mail: lpavic@irb.hr

Abstract

Solid-state impedance spectroscopy (SS-IS) was used to investigate the influence of structural modifications resulting from the addition of Nb_2O_5 on the dielectric properties and relaxation processes in the quaternary mixed glass former (MGF) system $35Na_2O–10V_2O_5–(55−x)P_2O_5–xNb_2O_5$ (x = 0–40, mol%). The dielectric parameters, including the dielectric strength and dielectric loss, are determined from the frequency and temperature-dependent complex permittivity data, revealing a significant dependence on the Nb_2O_5 content. The transition from a predominantly phosphate glass network ($x < 10$, region I) to a mixed niobate–phosphate glass network ($10 \leq x \leq 20$, region II) leads to an increase in the dielectric parameters, which correlates with the observed trend in the direct-current (DC) conductivity. In the predominantly niobate network ($x \geq 25$, region III), the highly polarizable nature of Nb^{5+} ions leads to a further increase in the dielectric permittivity and dielectric strength. This is particularly evident in Nb-40 glass-ceramic, which contains $Na_{13}Nb_{35}O_{94}$ crystalline phase with a tungsten bronze structure and exhibits the highest dielectric permittivity of 61.81 and the lowest loss factor of 0.032 at 303 K and 10 kHz. The relaxation studies, analyzed through modulus formalism and complex impedance data, show that DC conductivity and relaxation processes are governed by the same mechanism, attributed to ionic conductivity. In contrast to glasses with a single peak in frequency dependence of imaginary part of electrical modulus, $M''(\omega)$, Nb-40 glass-ceramic exhibits two distinct contributions with similar relaxation times. The high-frequency peak indicates bulk ionic conductivity, while the additional low-frequency peak is associated with the grain boundary effect, confirmed by the electrical equivalent circuit (EEC) modelling. The scaling characteristics of permittivity and conductivity spectra, along with the electrical modulus, validate time-temperature superposition and demonstrate a strong correlation with composition and modification of the glass structure upon Nb_2O_5 incorporation.

Keywords: phosphate glasses; glass-ceramics; impedance spectroscopy; dielectric properties; relaxation processes; permittivity scaling; conductivity scaling; modulus formalism

1. Introduction

The increasing energy demands of modern daily life and the rapid progress in the electronics industry have spurred the need for new sustainable and renewable materials suitable for electrical energy storage devices. These devices include solid-state batteries, electrostatic capacitors, electrochemical capacitors, etc. [1–4]. In the quest for efficient energy storage materials, significant focus has been directed towards inorganic materials, with a particular emphasis on oxide glasses and glass-ceramics. These materials possess dense and uniform microstructures with minimal grain boundaries making them highly desirable. Additionally, their compositions can be easily adjusted to achieve optimal properties, such as excellent structural and thermal stability and reliable energy storage performance.

Extensive research has been devoted to exploring niobate-based glass-(ceramic) systems, which show great promise for pulse power devices due to their tunable structure and high permittivity [5–8]. Indeed, Nb_2O_5 is known for its large electronic polarizability, and the structures of glass-(ceramic) compounds based on Nb_2O_5 are defined by the connectivity between off-centred NbO_6 octahedra. The distortion of these octahedra, resulting from shorter and longer Nb–O distances, offers structural flexibility that can lead to exceptional dielectric properties and the manifestation of ferroelectric behaviour [9]. Moreover, through controlled crystallization of Nb_2O_5-based glasses, it is possible to achieve the precipitation of ferroelectric crystalline phases with perovskite or tungsten bronze structures, resulting in materials exhibiting a high dielectric constant [10].

Research on the dielectric properties of Nb_2O_5-containing glass-ceramic systems has primarily focused on exploring various compositions based on the silicate network, such as $Na_2O–Nb_2O_5–SiO_2$ [11], $(Na_2O, K_2O)–Nb_2O_5–SiO_2–MO$ (M = Ca^{2+}, Sr^{2+}, Ba^{2+}) [12], and $Na_2O–Nb_2O_5–CaO–B_2O_3–SiO_2–ZrO_2$ [13], as well as the borate systems, including $Na_2O–Nb_2O_5–B_2O_3$ [14] and $BaO–Na_2O–Nb_2O_5–Al_2O_3–B_2O_3$ [7], and mixed borate-phosphate systems, in particular $K_2O–Na_2O–Nb_2O_5–B_2O_3–P_2O_5$ [12]. However, comparatively less attention has been given to predominantly phosphate-based glass-(ceramic) systems. Recent studies demonstrate that controlled crystallization of glasses from the $50Na_2O–xNb_2O_5–(50−x)P_2O_5$ system enables the preparation of glass-ceramics with a predominant fraction of the perovskite phase $NaNbO_3$ [15]. Notably, the glass-ceramic with the highest Nb_2O_5 content exhibits superior dielectric properties, characterized by a high dielectric constant and a low dielectric loss factor. Besides, the dielectric properties of the perovskite phase $NaNbO_3$ can be enhanced by mixing it with a glass with a composition $50Na_2O–25Nb_2O_5–25P_2O_5$, resulting in a composite material that serves as a promising dielectric candidate for energy storage capacitor ceramics [16]. Similar investigations were carried out on the glass-(ceramic) system $BaO–Na_2O–$

Nb$_2$O$_5$–WO$_3$–P$_2$O$_5$ with Ba$_2$NaNb$_5$O$_{15}$ and/or Ba$_2$Na$_4$W$_2$Nb$_8$O$_{30}$ crystalline phases with a tungsten bronze structure and the perovskite NaNbO$_3$ phase [17]. The glasses from this system were combined with Ba$_{0.85}$Ca$_{0.15}$Zr$_{0.10}$Ti$_{0.90}$O$_3$ (BCZT) ceramic [18], which is currently used as a dielectric material in the pulsed power capacitors industry due to its high dielectric permittivity [19]. Through this approach, a composite material that exhibits enhanced energy storage efficiency is developed.

Despite the encouraging findings obtained from the abovementioned investigations, there is a significant research gap in the literature regarding the characterization of the dielectric properties of niobate–phosphate (Nb–P) based glasses and glass-ceramics. Such mixed Nb–P-based glasses and glass-ceramics have been reported to manifest considerable promise for integration within electronic and optoelectronic technologies, as well as for biomedical applications [9]. Furthermore, regardless of solid-state impedance spectroscopy (SS-IS) being a powerful method for studying dielectric properties of various materials [20], only a few studies have reported investigations of the dielectric permittivity across a wide frequency and temperature range in Nb$_2$O$_5$-based glasses. To the best of our knowledge, the SS-IS investigations of the dielectric permittivity have been reported for glasses from the systems $(30-x)$M$_2$O–xNb$_2$O$_5$–70B$_2$O$_3$ (M = Li, Na) [21], 34.5A$_2$O–17.2Nb$_2$O$_5$–13.8WO$_3$–20.7P$_2$O$_5$–13.8B$_2$O$_3$ (A = Li, Na, K) [22], and 15K$_2$O–15Na$_2$O–xNb$_2$O$_5$–$(70-x)$P$_2$O$_5$ [23]. The cavity perturbation technique has recently been employed for studying the dielectric permittivity and loss of xLi$_2$O–xNb$_2$O$_5$–$(100-2x)$SiO$_2$ glasses [24]. However, these studies represent only a limited subset of the available literature on the topic.

In our previous study, we extensively studied an Nb–P-based glass system with a quaternary composition of 35Na$_2$O–10V$_2$O$_5$–$(55-x)$P$_2$O$_5$–xNb$_2$O$_5$ and conducted a comprehensive investigation into its thermal, (micro)structural, and electrical properties [25]. SS-IS measurements confirmed the mixed glass former (MGF) effect with the sample containing 20mol% Nb$_2$O$_5$ exhibiting the highest electrical conductivity attributed to the optimal interconnection between niobate and phosphate units, which facilitates the transport of Na$^+$ ions. Since our research group has demonstrated that SS-IS is a powerful method for investigating both the electrical and dielectric properties of phosphate-based glasses [26–27] and glass-ceramic materials [28–31] and it provides an effective approach for studying dielectric relaxation phenomena, gaining insights into the dielectric loss factor, and distinguishing between bulk and grain boundary components, we decided to investigate the dielectric properties and relaxation phenomena of the aforementioned 35Na$_2$O–10V$_2$O$_5$–$(55-x)$P$_2$O$_5$–xNb$_2$O$_5$ system.

This study focuses on the comprehensive analysis of the dielectric properties of the given system, encompassing an investigation of the complex permittivity, modulus, and impedance across a wide range of frequencies and temperatures. Through the examination of the permittivity data, the dielectric strength and loss factor are determined, revealing a strong influence of the Nb_2O_5 content on the dielectric properties. The scaling properties of permittivity are examined using the Summerfield scaling procedure, while the scaling properties of conductivity spectra are investigated using the Sidebottom scaling procedure. Relaxation studies are performed using modulus formalism and complex impedance data, and the findings demonstrate a strong correlation between the relaxation processes and DC conductivity. Among the studied samples, the glass-ceramic with 40mol% Nb_2O_5, which contains the $Na_{13}Nb_{35}O_{94}$ crystalline phase with a tungsten bronze structure [25], exhibits the highest permittivity and the lowest loss factor values. The results of this study thus demonstrate the significant potential of these materials as promising candidates for energy storage applications.

2. Methods

The glass-forming region (GFR) of the quaternary system $35Na_2O–10V_2O_5–(55−x)P_2O_5–xNb_2O_5$ has been thoroughly examined using the melt quenching method, and a detailed procedure for preparing the corresponding glass-(ceramic) samples is documented in Ref. [25]. The GFR displayed a relatively wide range, with Nb_2O_5 content extending up to 35mol%, while above the GFR, spontaneous crystallization occured, resulting in the formation of a partially crystallized (glass-ceramic) sample. It is worth noting that the samples are named according to the Nb_2O_5 content in the composition, where, for instance, Nb-20 glass indicates a sample containing 20mol% of Nb_2O_5. Furthermore, the aforementioned report includes an examination of diverse properties, such as density, molar volume, thermal behaviour, (micro)structural characteristics, and electrical properties [25]. These properties have been investigated using the following techniques: differential thermal analysis (DTA), powder X-ray diffraction (PXRD), scanning electron microscope equipped with an energy-dispersive X-ray spectroscopy (SEM-EDS), Raman spectroscopy, infrared attenuated total reflectance spectroscopy (IR-ATR), electron paramagnetic resonance (EPR), and solid-state impedance spectroscopy (SS-IS).

The investigation of the electrical and dielectric properties of the prepared samples was carried out using SS-IS. For electrical and dielectric property measurements, the samples were prepared as approximately 1 mm thick disks by cutting and polishing annealed samples. Gold electrodes with a diameter of 5.4 mm were then sputtered onto both

sides of the disks using the Sputter Coater SC7620. The dielectric and electrical properties were determined by measuring the complex impedance with an impedance analyzer (Novocontrol Alpha-AN Dielectric Spectrometer). These measurements were performed over a wide frequency range spanning from 0.01 Hz to 1 MHz, and within a temperature range of 183 to 523 K. Precise temperature control was maintained with an accuracy of ±0.20 K.

3. Results and discussion

3.1. Dielectric properties

The frequency dependence of the real and imaginary parts of the complex permittivity, $\varepsilon^*(\omega)$, at different temperatures for Nb-20 glass is shown in Fig. 1, as representative of all the studied samples. The complex permittivity is expressed as a complex number:

$$\varepsilon^*(\omega) = \frac{1}{i \cdot \omega \cdot C_0 \cdot Z^*} = \varepsilon'(\omega) - i\varepsilon''(\omega) \tag{1}$$

where $\varepsilon'(\omega)$ and $\varepsilon''(\omega)$ represent the frequency-dependent real and imaginary parts of the complex permittivity, and $\omega = 2\pi v$ represents the angular frequency, with v as the frequency. Capacitance of the empty cell in vacuum is $C_0 = \varepsilon_0 S/d$, where S represents the electrode area, d is the distance between the electrodes, and ε_0 stands for the vacuum permittivity. Frequency dependence of $\varepsilon'(\omega)$, known as a dielectric permittivity, seen from Fig. 1(a), exhibits two distinct characteristics arising from electrode polarization and bulk permittivity. The effect of electrode polarization is evident by the highest values of $\varepsilon'(\omega)$ observed at the lowest frequencies and the highest temperatures, and it arises due to the sample polarization caused by blocking gold electrodes, which restrict the transfer of mobile Na^+ ions into the external circuit. As the frequency increases, $\varepsilon'(\omega)$ decreases in a step-like manner due to dipole relaxation caused by the alignment of molecular dipoles under the applied field, i.e., rotational diffusion of dipoles in space, and it reaches a value known as the low-frequency plateau or static permittivity, ε_s, which is linked to the polarization processes of long-range hopping of mobile Na^+ ions within the structural network of the glass.
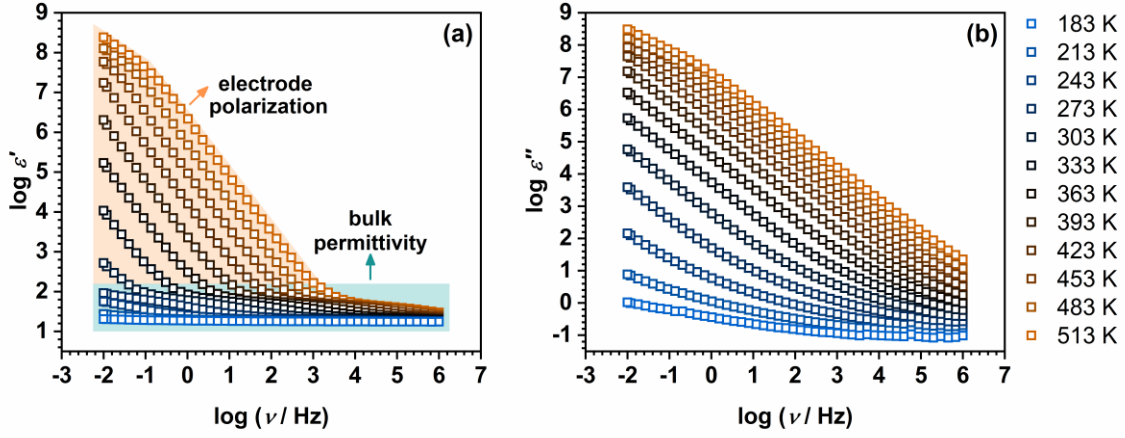
Fig. 1. Frequency dependence of (a) real and (b) imaginary parts of the complex permittivity at different temperatures for Nb-20 glass.

At the highest frequencies and lowest temperatures, $\varepsilon'(\omega)$ achieves a constant value, ε_∞, due to the fast polarization processes occurring in the glasses under the applied field, as the mobile ions are unable to rotate at a sufficient speed and their oscillation lags behind the applied field. On the other hand, $\varepsilon''(\omega)$ exhibits a decreasing trend with increasing frequency, as depicted in Fig. 1(b), owing to the translational diffusion process, namely, the long-range movement of mobile ions associated with DC conductivity [32]. The values of the $\varepsilon'(\omega)$ measured at 303 K and 10 kHz for the studied glasses-(ceramics) are given in Table 1, and they are found to increase with the addition of Nb_2O_5, with Nb-40 glass-ceramic exhibiting the highest value. The influence of Nb_2O_5 addition will be discussed next through the results of the low-frequency plateau analysis.

Table 1. Real component of permittivity, ε', and the dielectric strength, $\Delta\varepsilon$, for studied glasses at 303 K along with the relaxation frequencies, $\nu_{M''}$ and $\nu_{Z''}$, and times, $\tau_{M''}$ and $\tau_{Z''}$, determined from the frequency-dependent imaginary parts of modulus, $M''(\omega)$, and impedance $Z''(\omega)$, and the activation energies for the electrical modulus, $E_{M''}$, and impedance, $E_{Z''}$.

Sample	ε'^{a}	$\Delta\varepsilon'$	$\tau_{M''}$ / s	$\nu_{M''}$ / Hz	$E_{M''}$ / eV	$\tau_{Z''}$ / s	$\nu_{Z''}$ / Hz	$E_{Z''}$ / eV	tan δ^{a}
Nb-0	13.35	—	1.36×10^{-2}	11.73	0.74	2.04×10^{-2}	7.82	0.73	0.041
Nb-10	17.66	—	6.03×10^{-3}	26.40	0.68	1.36×10^{-2}	11.73	0.69	0.067
Nb-20	20.21	43.46	4.02×10^{-3}	39.60	0.65	9.04×10^{-3}	17.60	0.65	0.070

Nb-30	28.96	64.62	9.04×10^{-3}	17.60	0.65	2.04×10^{-2}	7.82	0.65	0.056
Nb-40	61.81	109.05	4.58×10^{-2}	3.48	0.65	1.03×10^{-1}	1.55	0.65	0.032

Note: [a] at $\nu = 10$ kHz

In certain glass systems, the low-frequency plateau can be masked as a result of significant electrode polarization, making it impossible to determine the static dielectric constant through experimental data. However, in the samples studied herein, the low-frequency plateau, ε_s, and high-frequency plateau, ε_∞, are clearly observable. To provide a clearer view of these plateaus, an enlarged representation of the spectra of the real component of permittivity is presented in Fig. 2(a). Since all analyzed samples exhibit a well-defined ε_s, it is possible to calculate the dielectric strength of relaxation using the equation $\Delta\varepsilon = \varepsilon_s - \varepsilon_\infty$, as proposed by Sidebottom [33–34]. This parameter characterizes the magnitude of bulk polarization, i.e., the polarization of the mobile ions in regards to the fixed glass matrix, and quantifies the rate of permittivity change due to the ionic relaxation. Calculated $\Delta\varepsilon$ values are listed in Table 1, while Fig. 2(b) illustrates the compositional and temperature dependence of $\Delta\varepsilon$ for all samples.
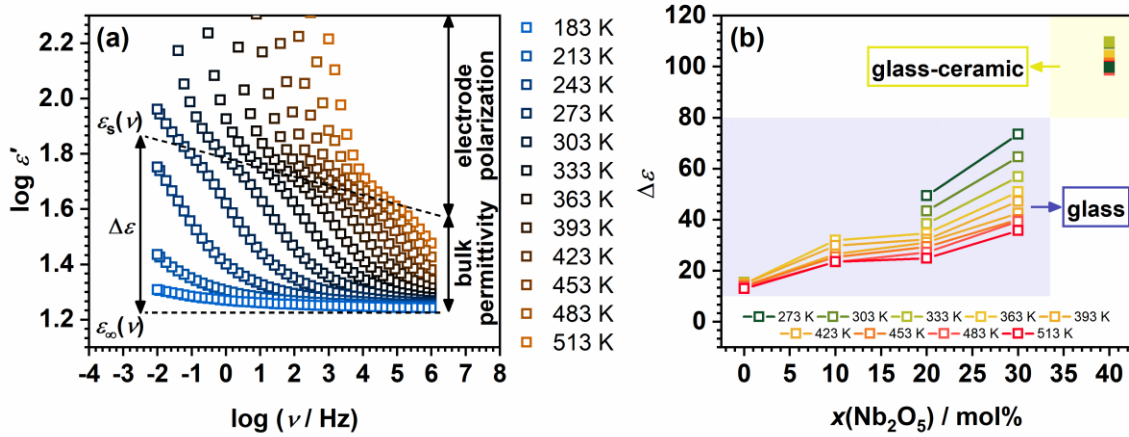

Fig. 2. (a) Enlarged view of frequency dependence of $\varepsilon'(\omega)$ at different temperatures for Nb-20 glass and (b) compositional and temperature dependence of $\Delta\varepsilon$ for all samples. The lines connecting data points are a guide to the eye.

$\Delta\varepsilon$ exhibits a gentle increase with the addition of Nb_2O_5 up to 20mol%, while further additions result in a significant jump in its values. In general, $\Delta\varepsilon$ is known to be influenced by ion hopping and, consequently, reflects variations in the dynamics of mobile ions that are closely linked to structural modifications of the glass network. It is interesting to note that the observed increasing trend closely resembles the trend observed for Sidebottom length, L,

7

described in our previous work [25]. Indeed, both $\Delta\varepsilon$ and L exhibit an increase in values in region I ($x < 10$), which follows the initial rise in DC conductivity. This increase is attributed to the enhanced mobility of Na^+ ions resulting from the depolymerization of the predominantly phosphate network upon the introduction of Nb_2O_5. In region II ($10 \le x \le 20$), where a mixed Nb–P glass network dominates, both L and $\Delta\varepsilon$ show only small changes as the DC conductivity continues to increase, which is consistent with the constant number density of Na^+ ions, $N_V(Na^+)$, and highlights the facilitated transport of Na^+ due to the optimal extent of the mixed glass network. However, further addition of Nb_2O_5 above 20mol% ($x \ge 25$, region III) leads to a substantial increase in $\Delta\varepsilon$, despite the decreasing trend in DC conductivity associated with the clustering of NbO_6 octahedra into a rigid 3D network which hampers the transport of Na^+ ions. As previously explained in the case of L, observed behaviour implies distinct ion dynamics on short- and long-range scales. Interestingly, the Nb-40 glass-ceramic exhibits the highest value of $\Delta\varepsilon$, which can be attributed to the significant concentration of highly polarizable Nb^{5+} ions [21,23]. Additionally, the presence of the $Na_{13}Nb_{35}O_{94}$ crystalline phase within the Nb-40 glass-ceramic [25], along with the polarization caused by the accumulation of space charge at the grain boundary interfaces, also contributes to the increase in $\Delta\varepsilon$ [22].

Another significant parameter that can be derived from the permittivity data is the loss factor, $\tan\delta$. It quantifies the phase difference resulting from energy loss within the sample at a specific frequency and is calculated as $\tan\delta = \varepsilon'(\omega)/\varepsilon''(\omega)$. Typically, dielectric losses are considerably lower at high frequencies compared to low frequencies and specific temperatures. This frequency-dependent behaviour of $\tan\delta$ is commonly associated with conduction losses and aligns with the observations made in the glass-(ceramic) samples studied in this research, as demonstrated in Fig. 3. Measured values for all samples at 303 K and 10 kHz are given in Table 1, while the inset in Fig. 3 depicts the compositional dependence of the loss factor. All samples exhibit low values of dielectric loss, with the Nb-40 glass-ceramic displaying the lowest value. Intriguingly, the compositional dependence of $\tan\delta$ closely correlates with the trend in DC conductivity, with Nb-20 glass exhibiting the maximum value, which is associated with its higher conductivity [25]. Based on these findings, it is apparent that $\varepsilon'(\omega)$ and $\tan\delta$ exhibit a significant dependence on the Nb_2O_5/P_2O_5 ratio, which is in accordance with previous research [15–16,35]. The increase in dielectric parameters resulting from the addition of Nb_2O_5 could thus be attributed to the favourable structural modifications that provide easy pathways for the movement of charges that contribute to the accumulation of space charge polarization [35].
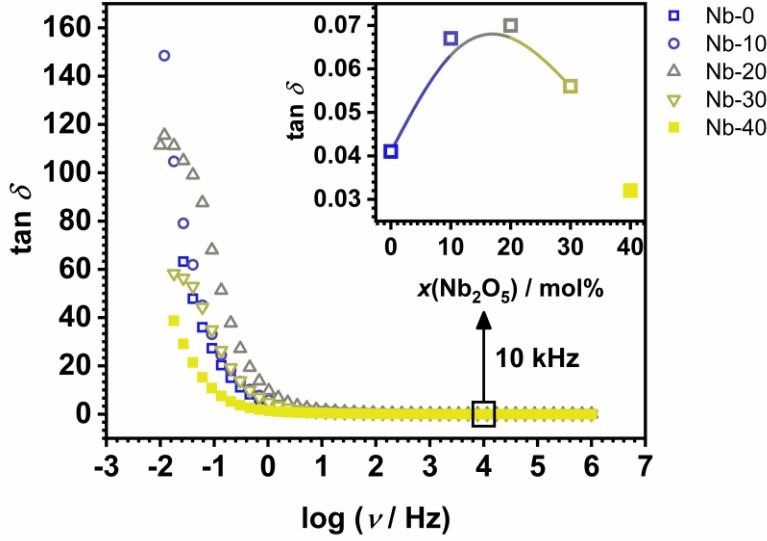
Fig. 3. Frequency dependence of loss factor, tan δ, for all samples at 303 K. Inset shows compositional dependence of tan δ for all samples at 303 K and 10 kHz. The lines connecting data points are a guide to the eye.

3.2. Scaling properties

Continuing the analysis, the scaling of permittivity spectra using the Summerfield scaling method is carried out. In this scaling, the y-axis is scaled by the product $(\varepsilon'(\omega) - \varepsilon_\infty)T$ [36], while the x-axis is scaled by the product of $T\sigma_{DC}$, where T represents temperature and σ_{DC} represents DC conductivity. Given that the complex conductivity, $\sigma^*(\omega)$, and complex permittivity, $\varepsilon^*(\omega)$, are mutually interrelated [37], and one value can be derived from the other, their spectra are expected to exhibit similar scaling properties. This is confirmed by the successful construction of master curves for all the studied glasses, as demonstrated in Fig. 4(a)–(d). However, it is evident that the shape of individual master curves differs. Just as individual conductivity master curves fail to overlap due to a change in shape [25], for the same reason, individual permittivity master curves cannot be successfully superimposed, see Fig. 4(e). The analysis excludes the Nb-40 sample due to its partial crystallization.
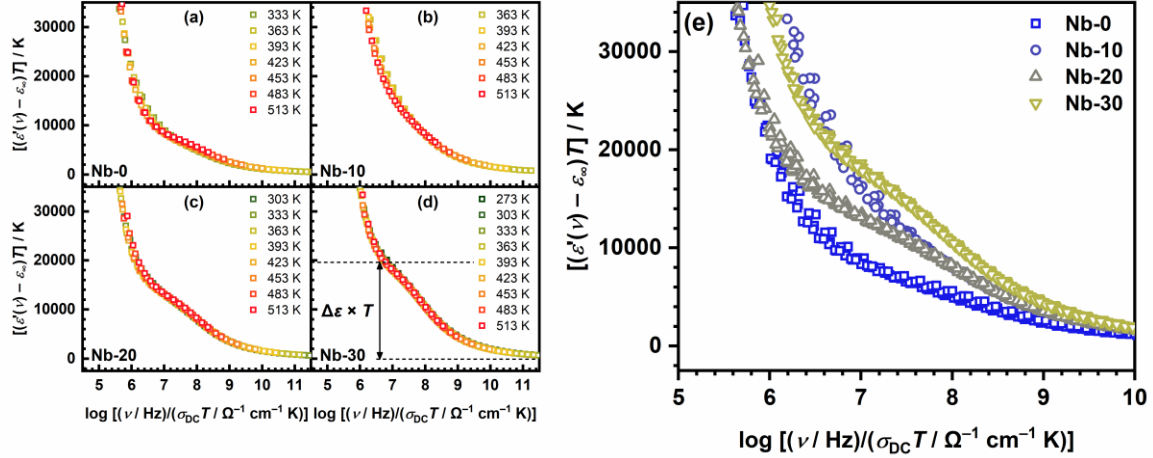
Fig. 4. Individual master curves of $\varepsilon'(\omega)$ for (a) Nb-0, (b) Nb-10, (c) Nb-20, and (d) Nb-30 glasses obtained using Summerfield scaling procedure and (e) superimposed master curves.

The prominence of ε_s varies among the glasses depending on the Nb_2O_5 content. Glasses with Nb_2O_5 content lower than 20mol% exhibit less pronounced ε_s, which gradually becomes more prominent as more Nb_2O_5 is added. This effect can be quantitatively described by the parameter $\Delta\varepsilon \times T$ derived from the scaled data, see Fig. 4(d), and is associated with the characteristic spatial extent of localized ion motions. In the glasses studied here, $\Delta\varepsilon \times T$ increases with the incorporation of Nb_2O_5, ranging from 5879 K for Nb-0 glass to 19596 K for Nb-30 glass. For Nb-10 and Nb-20 glasses, these values amount to 11598 and 13023 K, respectively, which align with the relatively small differences observed in ε' and $\Delta\varepsilon$ values between these two glasses, see Table 1. The increasing trend of $\Delta\varepsilon \times T$ follows the same pattern as previously explained for $\Delta\varepsilon$, progressively rising for samples with the highest Nb_2O_5 content, indicating strong dependence on both the composition and the degree of modification of the glass structure with Nb_2O_5. The initial increase in glasses with up to 20 mol% Nb_2O_5 contributes to favourable structural modifications, creating multiple channels that enhance ion transport and reduce Na^+ ion trapping, while in samples with the highest Nb_2O_5 content, the highly polarizable Nb^{5+} ions also contribute to this effect, resulting in further growth of $\Delta\varepsilon \times T$.

The presence of well-defined ε_s allows for expanding our investigation into scaling conductivity spectra. By utilizing the determined values of $\Delta\varepsilon$, we can scale conductivity spectra using the Sidebottom procedure [31]. This scaling procedure utilizes two scaling parameters, σ_{DC} and $\Delta\varepsilon$, and the expression for Sidebottom scaling is given by the equation $(\sigma'(\nu, T)/\sigma_{DC}(T)) = F(\varepsilon_0\Delta\varepsilon\nu/\sigma_{DC}(T))$, where σ' represents the real component of conductivity, ε_0 denotes the vacuum permittivity, and all other physical quantities retain their conventional interpretations. $\Delta\varepsilon$, influenced by

charge carrier relaxation, encompasses variations in charge carrier density and also the spatial extent of their diffusion. Therefore, this scaling technique is applicable universally and remains valid when the shape of the conductivity spectrum is independent of temperature.

Applying the Sidebottom scaling procedure results in perfect conductivity master curves for all the samples, providing evidence for the validity of time-temperature superposition (TTS). This observation suggests that the conduction mechanism remains unchanged despite temperature variations, aligning with the successful application of Summerfield scaling in our previous research [25]. However, when attempting to superimpose the individual master curves obtained by the Sidebottom method in the super-scaling procedure, as depicted in Fig. 5(a), they do not overlap, similar to the case with the master curves obtained by the Summerfield method.
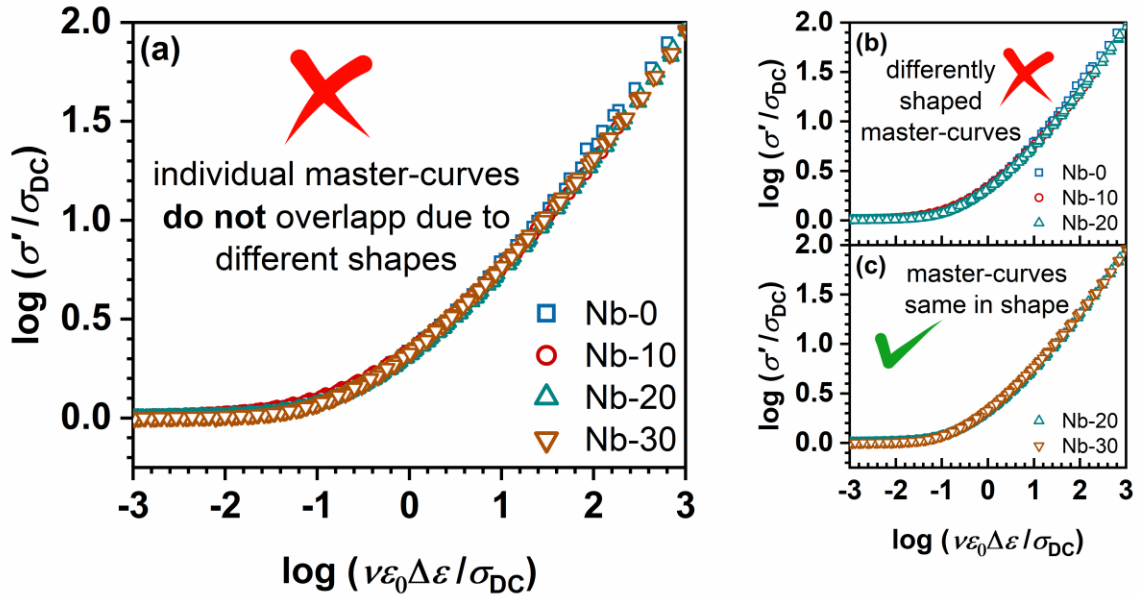

Fig. 5. Construction of (a) super master curve of the conductivity isotherms obtained by applying the Sidebottom scaling procedure for all glasses, (b) differently shaped master curves of Nb-0, Nb-10, and Nb-30 glasses, and (c) master curves of Nb-20 and Nb-30 glasses same in shape.

Moreover, the shape of master curves for glasses with $0 \leq x \leq 20$ distinctly varies, see Fig. 5(b), whereas it remains consistent for glasses with $20 \leq x \leq 30$, see Fig. 5(c), just as observed in the case of Summerfield scaling [25]. Since conventional MGF systems do not exhibit a change in the shape of master curves, the findings of our study further contribute to the understanding that a mixed P-TMO network has a more intricate influence on the transport of Na^+

ions, providing different structural energy landscapes for Na^+ conduction pathways. In the following section, relaxation studies using modulus formalism and complex impedance are presented.

3.3. Relaxation studies

Returning to the permittivity data, it is important to consider that electrical relaxation processes in glasses can be affected by high capacitance effects, such as electrode polarization. As previously shown in Fig. 1(b), relaxation peaks are not visible in the $\varepsilon''(\omega)$ representation, which is consistent with the usual behaviour observed in materials containing mobile ions. Therefore, an alternative approach for analyzing the electrical relaxation behaviour in glasses is to use the electrical modulus model [38]. This model defines modulus, $M^*(\omega)$, as reciprocal of $\varepsilon^*(\omega)$:

$$M^*(\omega) = \frac{1}{\varepsilon^*(\omega)} = \frac{\varepsilon'(\omega)}{\varepsilon'(\omega)^2 + \varepsilon''(\omega)^2} + \frac{i\varepsilon''(\omega)}{\varepsilon'(\omega)^2 + \varepsilon''(\omega)^2} = M'(\omega) + iM''(\omega) \qquad (2)$$

Fig. 6 illustrates the frequency-dependent behaviour of the real, $M'(\omega)$, and imaginary, $M''(\omega)$, components of the electrical modulus for Nb-10 glass at different temperatures.
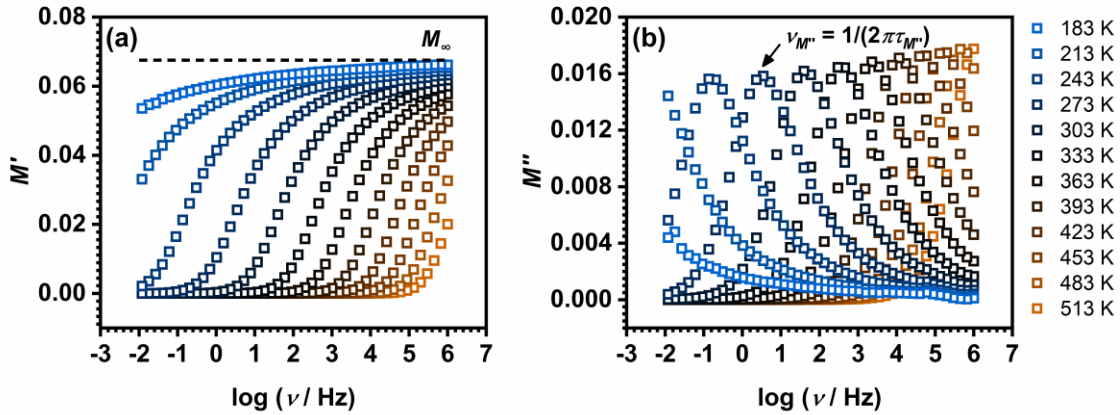

Fig. 6. Frequency dependence of the (a) real part, $M'(\omega)$, and (b) imaginary part, $M''(\omega)$, of electrical modulus at different temperatures for Nb-10 glass.

While $M'(\omega)$ shows a sigmoidal increasing trend with increasing frequency, eventually reaching a plateau corresponding to the limiting value of M_∞, the frequency dependence of $M''(\omega)$ is characterized by a distinct maximum that occurs at a specific frequency known as the relaxation frequency, $v_{M''}$. With increasing temperature, this maximum shifts towards higher frequencies which indicates the temperature dependence of electrical relaxation. The peak maximum separates two distinct relaxation regions, one located above and the other below it. In the low-frequency

region ($v < v_{M''}$), charge carriers demonstrate enhanced mobility over longer distances. On the other hand, in the higher-frequency region ($v > v_{M''}$), the relaxation polarization process occurs, confining charge carriers to potential wells and limiting their mobility to shorter distances. Based on a given value of $v_{M''}$, the relaxation time, $\tau_{M''}$, can be calculated as the reciprocal according to the equation $\tau_{M''} = 1/(2\pi v_{M''})$. Table 1 provides the corresponding $\tau_{M''}$ values for all samples at 303 K, and their values will be addressed subsequently.

The TTS analysis can also be performed with electrical modulus data to investigate whether the relaxation process remains consistent across the studied compositions and temperature range. In this approach, the normalized imaginary part of the electrical modulus, $M''(\omega)/M''(\omega)_{max}$, is plotted as a function of $v_{M''}/v_{M'',max}$. As shown in Fig. 7(a)–(c), the successful construction of master curves is achieved for all the samples, and when superimposed, they collapse into a single super master curve, seen from Fig. 7(a). Nb-40 glass-ceramic is excluded from the super scaling procedure due to the presence of an additional relaxation process, seen from Fig. 7(c).
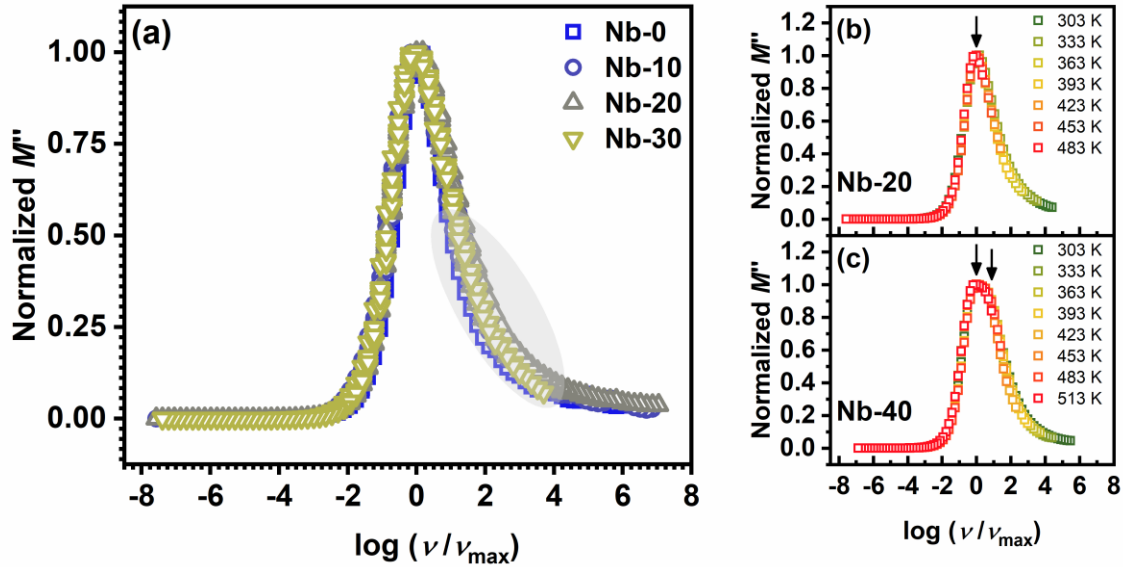

Fig. 7. (a) Superimposed master curves of $M''(\omega)$ for all glasses and comparison of individual master curves for (b) Nb-20 glass as a representative for all glasses and (c) Nb-40 glass-ceramic.

The super master curve reveals two distinct regions, one below the $M''(\omega)$ peak, where DC conductivity dominates and all data points lie on the curve, and another above the $M''(\omega)$ peak, which corresponds to the decay of the electric field, where ions are confined to potential wells and can move freely within those wells. However, a slight deviation from the super master curve is observed at high frequencies and it could be attributed to the effects of short-

13

time dynamics which involves relaxation movements or adjustments of the glass network influenced by the local structural factors. Similar scaling behaviour has been observed in other glass systems [26], and it may be related to the incorporation of niobate units into the glass network which leads to a more constrained local environment and causes dispersion in the shorter time region. Hence, the deviations observed in the scaled data for these glasses could be attributed to variations in the distribution of relaxation times caused by the presence of structural disorder in the glass network.

The exploration of the relaxation mechanism in all samples also includes the analysis of the imaginary part of impedance, $Z''(\omega)$, seen from Fig. 8(a)–(b). Similar to $M''(\omega)$, $Z''(\omega)$ exhibits a temperature-dependent maximum at a specific frequency, and its reciprocal value represents the time required for dipole reorientation. However, unlike the electrical modulus, which is dominated by processes exhibiting the lowest capacitance values, the frequency dependence of $Z''(\omega)$ showcases processes exhibiting the highest resistance values. By examining the maximum of $Z''(\omega)$, the relaxation times, $\tau_{Z''}$, at various temperatures can be calculated using equation $\tau_{Z''} = 1/(2\pi\nu_{Z''})$ and obtained values are presented in Table 1.
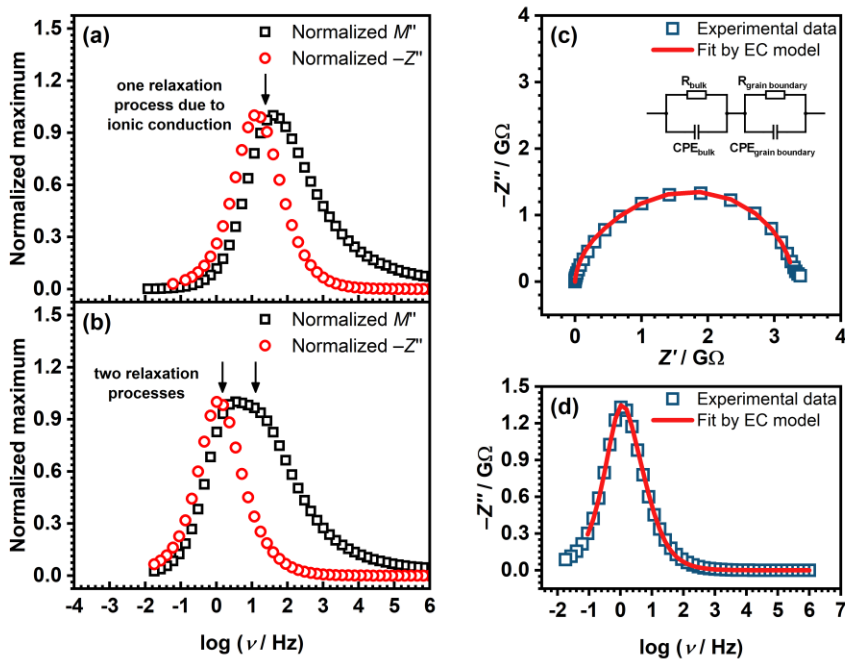

Fig. 8. Frequency dependence of normalized $M''(\omega)$ and $Z''(\omega)$ curves for (a) Nb-20 glass and (b) Nb-40 glass-ceramic, and equivalent circuit modelling of (c) complex impedance and (d) frequency dependence of $Z''(\omega)$ at 303 K for Nb-40 glass-ceramic.

Furthermore, to investigate whether the observed maxima in the frequency dependence curves of $M''(\omega)$ and $Z''(\omega)$ correspond to the same relaxation process, the curves are normalized, as presented in Fig. 8(a) and (b). Indeed, the maxima of both $M''(\omega)$ and $Z''(\omega)$ curves are closely aligned for all glasses, seen from Fig. 8(a), yet they do not entirely overlap, indicating a distribution of relaxation times and contributions from both localized and long-range relaxation processes. Comparing the extracted values of $v_{M''}$ and $v_{Z''}$, as well as $\tau_{M''}$ and $\tau_{Z''}$, seen from Table 1, it is found that the values are similar and exhibit equal non-monotonic trends, with relaxation frequencies reaching a maximum for Nb-20 glass, whereas relaxation times show a minimum for Nb-20 glass, regardless of whether they are obtained from the maxima of $M''(\omega)$ or $Z''(\omega)$. This suggests that the observed phenomenon represents the same underlying process.

In contrast to glasses from this study, Nb-40 glass-ceramic is a heterogeneous system composed of uniformly distributed crystalline grains within a glassy matrix [25] and thus shows different results. As mentioned earlier, the frequency dependence of $M''(\omega)$ for Nb-40 reveals contributions from two relaxation processes whose maxima overlap due to similar relaxation frequencies, whereas $Z''(\omega)$ exhibits a single maximum which closely aligns with the first of the two maxima in the $M''(\omega)$ curve, seen from Fig. 8(b). Since $Z''(\omega)$ highlights processes characterized by the highest resistance values, the presence of only one maximum in $Z''(\omega)$ indicates that the dominant process occurring at a lower frequency exhibits higher resistance values compared to the process observed at a higher frequency and as a result, it is masked. Considering the substantial amount of the crystalline $Na_{13}Nb_{35}O_{94}$ (33wt%) in Nb-40 glass-ceramic [25], the low-frequency contribution is likely due to the grain boundary, while the higher-frequency process is attributed to the bulk response, as confirmed by the electrical equivalent circuit (EEC) modelling. The EEC used to represent the bulk and grain boundary phenomena in Nb-40 glass-ceramic consists of two parallel combinations of the the resistor (R) and and a constant phase element (CPE). As illustrated in Fig. 8(c) and (d), the experimental data show excellent agreement with the theoretical curves. The obtained capacitance values for both relaxation processes fall within the range of 10^{-11} F and are associated with significant bulk fraction and grain boundaries [28–30,39]. On the other hand, the resistance values of the bulk and the grain boundary differ by an order of magnitude, with the resistance of the grain boundary contribution being on the order of 10^9, which is consistent with the results of relaxation studies.

Back to the values of relaxation frequencies and times determined from $M''(\omega)$ and $Z''(\omega)$, by examining the slope of the logarithm of $v_{M''}$ and $v_{Z''}$ plotted against $1000/T$, it is possible to determine the activation energies for the electrical modulus, $E_{M''}$, and impedance, $E_{Z''}$. It is interesting to compare the obtained activation energy values with

the activation energy for DC conduction, E_{DC}, from our previous work [25]. As depicted in Fig. 9(a), these values show a remarkable similarity, confirming the agreement between the relaxation processes and DC conductivity.
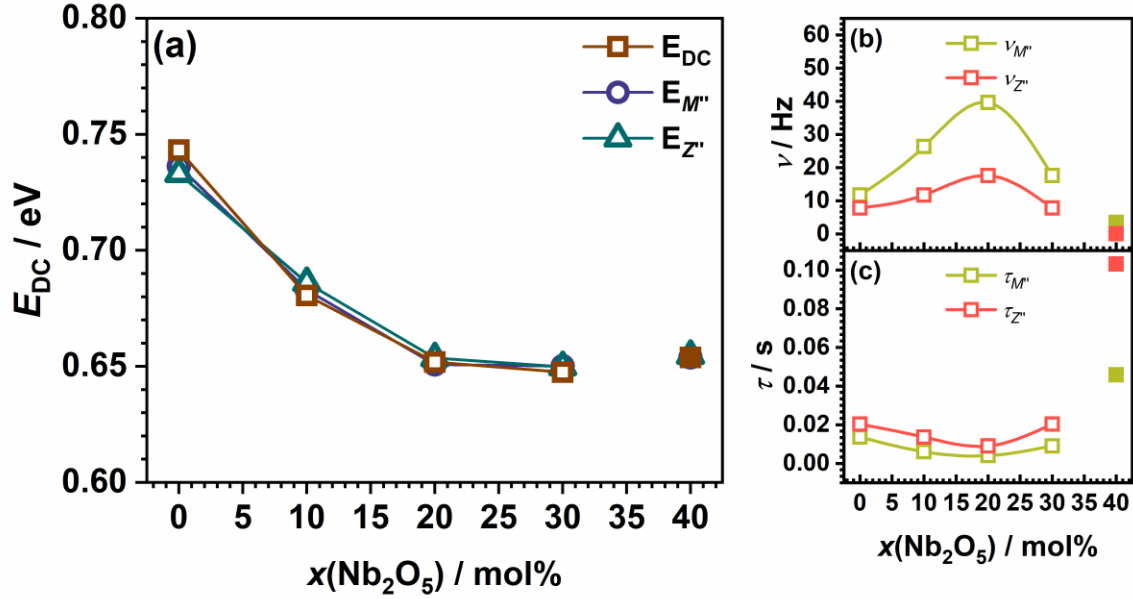

Fig. 9. (a) Comparison of activation energies for σ_{DC}, $M''(\omega)$, and $Z''(\omega)$ and compositional dependence of (b) relaxation frequencies and (c) relaxation times determined from the maxima of $M''(\omega)$ and $Z''(\omega)$ for all samples. The lines connecting data points are a guide to the eye.

This behaviour provides further confirmation of the existence of a single conduction mechanism, where the same activation energies are associated with the same relaxation process. What's more, the compositional dependence of relaxation frequencies, seen from Fig. 9(b), clearly reflects the non-monotonic trend observed in DC conductivity [25], with the highest value corresponding to Nb-20 glass. Consequently, this glass sample exhibits the lowest relaxation time, seen from Fig. 9(c), which results in the highest conductivity among the glasses studied. Additionally, the activation energies corresponding to the relaxation processes attributed to bulk and grain boundary contributions in Nb-40 glass-ceramics are found to be equal based on the analysis of modulus data.

To visualize the observed relaxation process, it is interesting to compare the electrical modulus and conductivity spectra at a given temperature, as shown in Fig. 10.
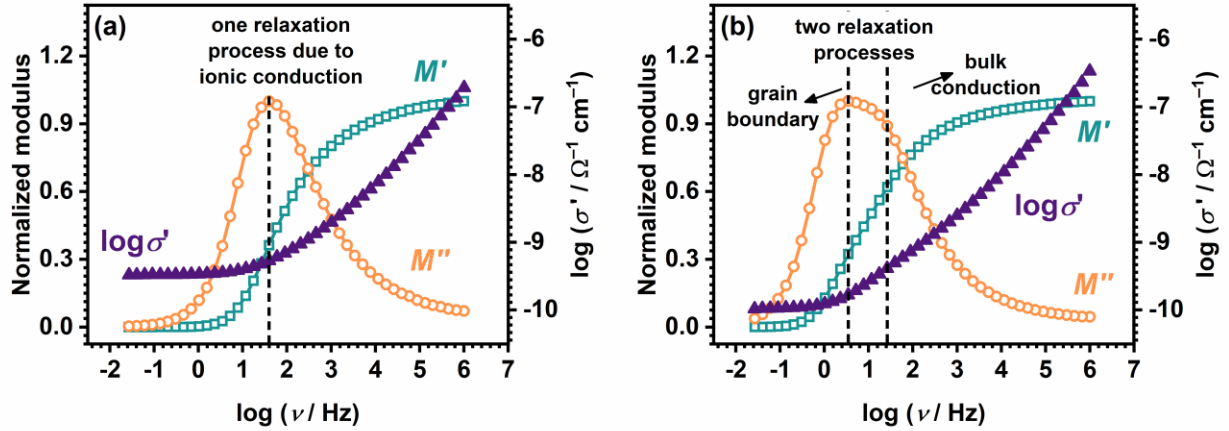
Fig. 10. Comparison of frequency dependences of $M'(\omega)$, $M''(\omega)$, and $\sigma'(\omega)$ at 303 K for (a) Nb-20 glass and (b) Nb-40 glass-ceramic.

It can be observed that all glasses exhibit a single relaxation process, which is manifested as a peak in $M''(\omega)$, and it coincides with the onset of dispersion in the conductivity spectrum. The position of the peak maximum in $M''(\omega)$ corresponds to the inflexion point in the frequency dependence of $M'(\omega)$, and the intersection of the two curves at the point of maximum corresponds to the characteristic relaxation frequency $\nu_{M''}$. While glasses show only one peak due to bulk ionic conduction, the conductivity spectrum and frequency dependence of $M''(\omega)$ of Nb-40 glass-ceramic reveal two contributions, with the additional low-frequency peak corresponding to the contribution of the grain boundary.

4. Conclusion

This study elucidates the influence of structural modifications arising from the substitution of P_2O_5 with Nb_2O_5 on the dielectric properties and relaxation processes in the quaternary MGF glass-(ceramic) series $35Na_2O–10V_2O_5–(55−x)P_2O_5–xNb_2O_5$ ($x = 0–40$, mol%). Our findings reveal that the dielectric parameters, including the dielectric permittivity, dielectric strength, and dielectric loss, exhibit a strong dependence on the Nb_2O_5 content, as determined from the frequency and temperature-dependent complex permittivity data. The dielectric properties are influenced by the MGF effect in a similar manner as it affects the previously reported conductivity of the studied system. This relationship is particularly evident in the compositional dependence of the dielectric strength, which is influenced by ion hopping and reflects changes in the dynamics of mobile ions associated with structural modifications of the glass network. Similar to the observed trend in DC conductivity, the variation in dielectric strength also shows an initial

17

increase in region I ($x < 10$) attributed to the enhanced mobility of Na^+ ions resulting from the depolymerization of the predominantly phosphate network, which is induced by the addition of Nb_2O_5. Furthermore, in the region II of a mixed dominant Nb–P glass network ($10 \leq x \leq 20$), the variation in dielectric strength exhibits minimal changes, which is consistent with the constant number density of Na^+ ions and indicates that the mixed glass network efficiently facilitates the transport of Na^+ ions. However, in the region III of a predominantly niobate network ($x \geq 25$), the influence of the highly polarizable nature of Nb^{5+} ions prevails over the dielectric strength, and it continues to increase with an increase in the Nb_2O_5 content. Nb-40 glass-ceramic exhibits the highest dielectric strength and the lowest loss factor, which is attributed to two factors: the large polarizability of Nb^{5+} ions and the polarization resulting from the accumulation of space charge at the grain boundary interfaces. The relaxation studies, conducted through the analysis of modulus formalism and complex impedance data, indicate that the DC conductivity and relaxation processes are associated with the same underlying relaxation mechanism, which is attributed to ionic conductivity. Unlike glasses that show only one peak resulting from DC conductivity, the conductivity spectra and frequency dependence of $M''(\omega)$ in Nb-40 glass-ceramic reveal two distinct contributions with similar relaxation times. The high-frequency peak corresponds to ionic conductivity in the bulk component, while the additional low-frequency peak corresponds to the contribution from the grain boundary, as confirmed by EEC modelling. The scaling characteristics observed in the permittivity and conductivity spectra, along with the electrical modulus, confirm the applicability of time-temperature superposition and unveil a strong correlation with both the composition and the degree of modification of the glass structure upon Nb_2O_5 incorporation.

Acknowledgements

Conflict of Interest

The authors declare that they have no known competing financial/commercial interests or personal relationships that could have appeared to influence the work reported in this paper.

References

[1] Q.B. Yuan, M. Chen, S.L. Zhan, Y.X. Li, Y. Lin, and H.B. Yang, Ceramic-based dielectrics for electrostatic energy storage applications: Fundamental aspects, recent progress, and remaining challenges, *Chem. Eng. J.*, 446(2022), art. No. 136315.

[2] Z.H. Yao, Z. Song, H. Hao, *et al.*, Homogeneous/inhomogeneous-structured dielectrics and their energy-storage performances, *Adv. Mater.*, 29(2017), No. 20, art. No. 1601727.

[3] A. Smirnova, A. Numan-Al-Mobin, and Inamuddin, *Green Sustainable Process for Chemical and Environmental Engineering and Science: Solid-State Energy Storage - A Path to Environmental Sustainability*, Elsevier, Amsterdam, 2023.

[4] S. Gandi, V.S.C.S. Vaddadi, S.S.S. Panda, *et al.*, Recent progress in the development of glass and glass-ceramic cathode/solid electrolyte materials for next-generation high capacity all-solid-state sodium-ion batteries: A review, *J. Power Sources*, 521(2022), art. No. 230930.

[5] C. Chen, Y.X. Zheng, and B. Li, Achieving ultrafast discharge speed and excellent energy storage efficiency in environmentally friendly niobate-based glass ceramics, *J. Eur. Ceram. Soc.*, 42(2022), No. 15, p. 6977.

[6] T.T. Fu, S.F. Xie, C.S. Liu, H.R. Bai, B. Shen, and J.W. Zhai, High discharge energy density and ultralow dielectric loss in alkali-free niobate-based glass-ceramics by composition optimization, *Scripta Mater.*, 221(2022), art. No. 114993.

[7] F. Luo, Y.Y. Qin, F. Shang, and G.H. Chen, Crystallization temperature dependence of structure, electrical and energy storage properties in $BaO–Na_2O–Nb_2O_5–Al_2O_3–B_2O_3$ glass ceramics, *Ceram. Int.*, 48(2022), No. 20, p. 30661.

[8] C.S. Liu, S.F. Xie, K.K. Chen, B.J. Song, B. Shen, and J.W. Zhai, High breakdown strength and enhanced energy storage performance of niobate-based glass-ceramics via glass phase structure optimization, *Ceram. Int.*, 47(2021), No. 22, p. 31229.

[9] T. Komatsu, T. Honma, T. Tasheva, and V. Dimitrov, Structural role of Nb_2O_5 in glass-forming ability, electronic polarizability and nanocrystallization in glasses: A review, *J. Non-Cryst. Solids*, 581(2022), art. No. 121414.

[10] S.J. Wang, J. Tian, K. Yang, J.R. Liu, J.W. Zhai, and B. Shen, Crystallization kinetics behavior and dielectric energy storage properties of strontium potassium niobate glass-ceramics with different nucleating agents, *Ceram. Int.*, 44(2018), No. 7, p. 8528.

[11] M.P.F. Graça, M.G.F. da Silva, A.S.B. Sombra, and M.A. Valente, Electric and dielectric properties of a SiO_2–Na_2O–Nb_2O_5 glass subject to a controlled heat-treatment process, *Physica B*, 396(2007), No. 1-2, p. 62.

[12] X. Peng, Y.P. Pu, Z.X. Sun, *et al.*, Achieving high electrical homogeneity in (Na_2O, K_2O)–Nb_2O_5–SiO_2–MO (M = Ca^{2+}, Sr^{2+}, Ba^{2+}) glass-ceramics for energy storage by composition design, *Composites Part B*, 260(2023), art. No. 110765.

[13] X.Y. Liu, K. Zhao, and H. Jiao, Stabilizing the anti-ferroelectric phase in NaO–Nb_2O_5–CaO–B_2O_3–SiO_2–ZrO_2 glass-ceramics using the modification of K^+ ion, *Ceram. Int*., 49(2023), No. 12, p. 21078.

[14] M.P.F. Graça, M.G.F. da Silva, and M.A. Valente, $NaNbO_3$ crystals dispersed in a B_2O_3 glass matrix – Structural characteristics versus electrical and dielectrical properties, *Solid State Sci*., 11(2009), No. 2, p. 570.

[15] S. Benyounoussy, L. Bih, F. Muñoz, F. Rubio-Marcos, M. Naji, and A. El Bouari, Structure, dielectric, and energy storage behaviors of the lossy glass-ceramics obtained from Na_2O–Nb_2O_5–P_2O_5 glassy-system, *Phase Transitions*, 94(2021), No. 9, p. 634.

[16] S. Benyounoussy, L. Bih, F. Muñoz, F. Rubio-Marcos, and A. El Bouari, Effect of the Na_2O–Nb_2O_5–P_2O_5 glass additive on the structure, dielectric and energy storage performances of sodium niobate ceramics, *Heliyon*, 7(2021), No. 5, art. No. e07113.

[17] A. Ihyadn, A. Lahmar, D. Mezzane, *et al.*, Structural, electrical and energy storage properties of BaO–Na_2O–Nb_2O_5–WO_3–P_2O_5 glass-ceramics system, 6(2019), art. No. 115203

[18] A. Ihyadn, S. Merselmiz, D. Mezzane, *et al.*, Dielectric and energy storage properties of $Ba_{0.85}Ca_{0.15}Zr_{0.1}Ti_{0.90}O_3$ ceramics with BaO–Na_2O–Nb_2O_5–WO_3–P_2O_5 glass addition, *J. Mater. Sci. Mater. Electron*., 34(2023), No. 12, art. No. 1051.

[19] M. Maraj, W.W. Wei, B.L. Peng, and W.H. Sun, Dielectric and energy storage properties of $Ba_{(1-x)}Ca_xZr_yTi_{(1-y)}O_3$ (BCZT): A review, *Materials*, 12(2019), No. 21, art. No. 3641.

[20] L. Zhang, Y.P. Pu, and M. Chen, Complex impedance spectroscopy for capacitive energy-storage ceramics: A review and prospects, *Mater. Today Chem*., 28(2023), art. No. 101353.

[21] S. Sanghi, A. Sheoran, A. Agarwal, and S. Khasa, Conductivity and dielectric relaxation in niobium alkali borate glasses, *Physica B*, 405(2010), No. 24, p. 4919.

[22] M.P.F. Graça, B.M.G. Melo, P.R. Prezas, M.A. Valente, F.N.A. Freire, and L. Bih, Electrical and dielectric analysis of phosphate based glasses doped with alkali oxides, *Mater. Des*., 86(2015), p. 427.

[23] Y. Attafi and S.Q. Liu, Conductivity and dielectric properties of Na_2O–K_2O–Nb_2O_5–P_2O_5 glasses with varying amounts of Nb_2O_5, *J. Non-Cryst. Solids*, 447(2016), p. 74.

[24] K.S. Gerace, M.T. Lanagan, and J.C. Mauro, Dielectric polarizability of SiO_2 in niobiosilicate glasses, *J. Am. Ceram. Soc.*, 106(2023), No. 8, p. 4546.

[25] S. Marijan, M. Razum, T. Klaser, *et al.*, Tailoring structure for improved sodium mobility and electrical properties in V_2O_5–Nb_2O_5–P_2O_5 glass(es)-(ceramics), *J. Phys. Chem. Solids*, 181(2023), art. No. 111461.

[26] A. Moguš-Milanković, K. Sklepić, H. Blažanović, P. Mošner, M. Vorokhta, and L. Koudelka, Influence of germanium oxide addition on the electrical properties of Li_2O–B_2O_3–P_2O_5 glasses, *J. Power Sources*, 242(2013), p. 91.

[27] V. Prasad, L. Pavić, A. Moguš-Milanković, *et al.*, Influence of silver ion concentration on dielectric characteristics of Li_2O–Nb_2O_5–P_2O_5 glasses, *J. Alloys Compd.*, 773(2019), p. 654.

[28] L. Pavić, Ž. Skoko, A. Gajović, D.S. Su, and A. Moguš-Milanković, Electrical transport in iron phosphate glass-ceramics, *J. Non-Cryst. Solids*, 502(2018), p. 44.

[29] L. Pavić, K. Sklepić, Ž. Skoko, *et al.*, Ionic conductivity of lithium germanium phosphate glass-ceramics, *J. Phys. Chem. C*, 123(2019), No. 38, p. 23312.

[30] L. Pavić, J. Nikolić, M.P.F. Graça, *et al.*, Effect of controlled crystallization on polaronic transport in phosphate-based glass-ceramics, *Int. J. Appl. Glass Sci.*, 11(2020), No. 1, p. 97.

[31] A. Bafti, S. Kubuki, H. Ertap, *et al.*, Electrical transport in iron phosphate-based glass-(ceramics): Insights into the role of B_2O_3 and HfO_2 from model-free scaling procedures, *Nanomaterials*, 12(2022), No. 4, art. No. 639.

[32] F. Kremer and A. Schönhals, *Broadband Dielectric Spectroscopy*, Springer Berlin, Heidelberg, 2003.

[33] D.L. Sidebottom, Universal approach for scaling the ac conductivity in ionic glasses, *Phys. Rev. Lett.*, 82(1999), No. 18, p. 3653.

[34] D.L. Sidebottom, B. Roling, and K. Funke, Ionic conduction in solids: Comparing conductivity and modulus representations with regard to scaling properties, *Phys. Rev. B*, 63(2000), No. 2, art. No. 024301.

[35] N.K. Mohan, M.R. Reddy, C.K. Jayasankar, and N. Veeraiah, Spectroscopic and dielectric studies on MnO doped PbO–Nb_2O_5–P_2O_5 glass system, *J. Alloys Compd.*, 458(2008), No. 1-2, p. 66.

[36] B. Roling, Scaling properties of the conductivity spectra of glasses and supercooled melts, *Solid State Ion.*,

105(1998), No. 1-4, p. 185.

[37] M. Bakry and L. Klinkenbusch, Using the Kramers-Kronig transforms to retrieve the conductivity from the effective complex permittivity, *Adv. Radio Sci.*, 16(2018), p. 23.

[38] P.B. Macedo, C.T. Moynihan, and R. Bose, Role of ionic diffusion in polarization in vitreous ionic conductors, *Phys. Chem. Glasses*, 13(1972), No. 6, p. 171.

[39] D.C. Sinclair, Characterization of electro-materials using ac impedance spectroscopy, *Bol. Soc. Esp. Ceram. Vidrio*, 34(1995), No. 2, p. 55.